High Resolution Shape Completion Using Deep Neural Networks for Global Structure and Local Geometry Inference
(Supplementary Material)

Xiaoguang Han[1,*] Zhen Li[1,*] Haibin Huang[2] Evangelos Kalogerakis[2] Yizhou Yu[1]
[1]The University of Hong Kong [2]University of Massachusetts, Amherst

1. Visualization of Input

As shown in Fig. 1, each point cloud is converted into a signed distance field and represented as both a Colored SDF (CSDF) and a binary surface (BSurf). We show an example for each of them by sampling a cross section from a 256^3 voxelized representation. We also show two sampled projected depth images.

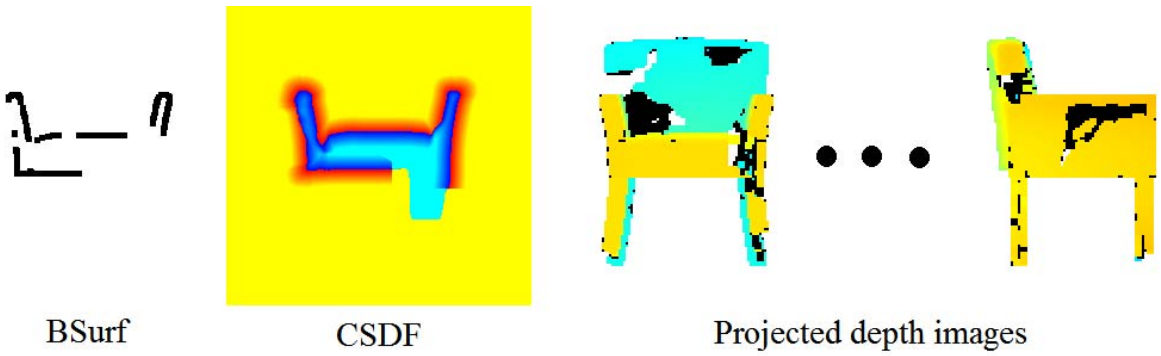

Figure 1. Visualization for CSDF+BSurf representation generated from input point cloud and the colored projected depth images.

[*]equal contribution

2. Sampled Outputs of Global Structure Prediction

Fig. 2 shows a gallery of outputs from our global structure inference network only. We show two results from each object category.

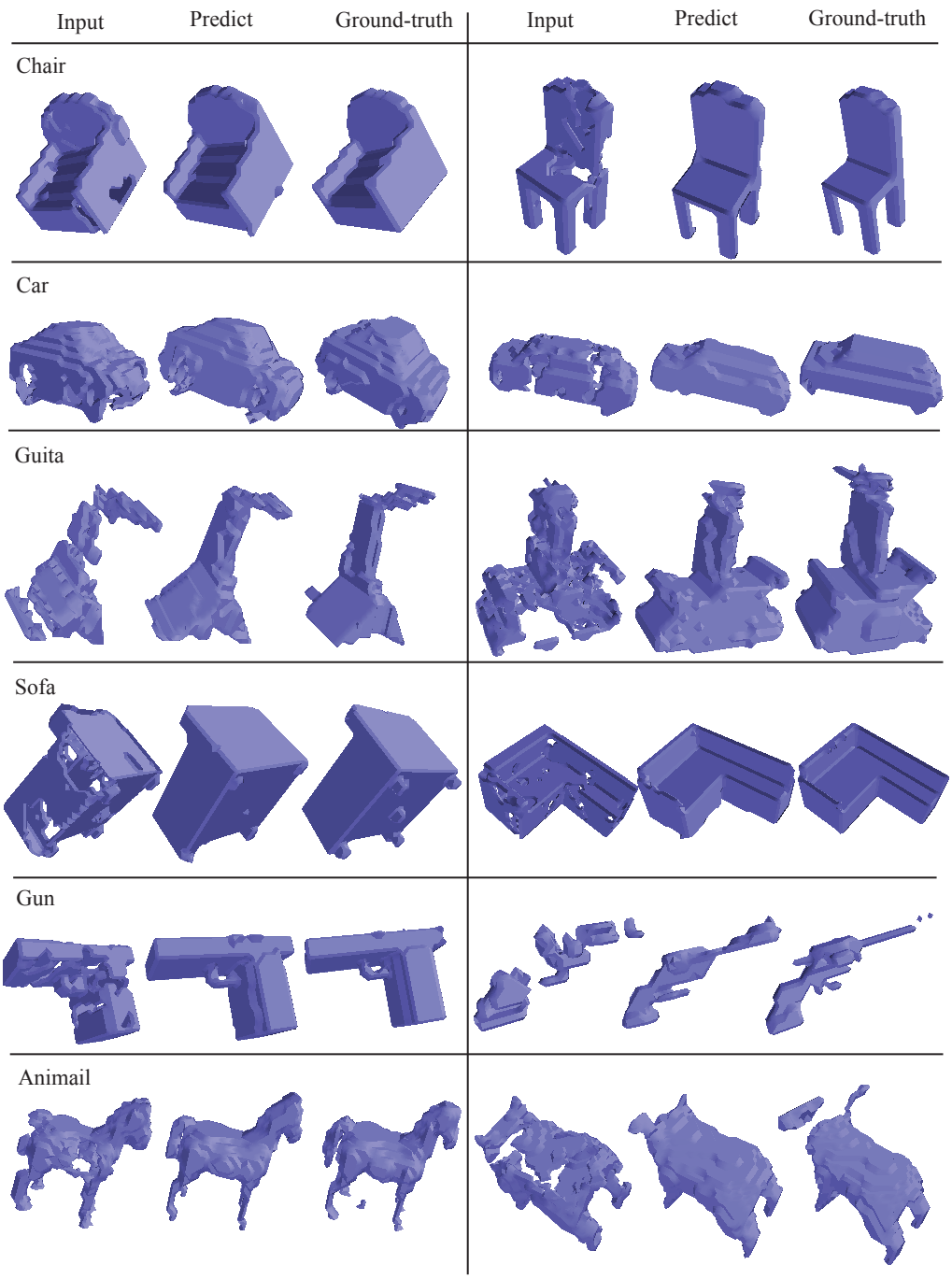

Figure 2. Sampled outputs from our global structure inference only. Two models are shown per category. For each model, the input, predicted global structure and ground-truth structure are shown side by side.

3. Sampled Outputs from Ablation Study of Global Structure Prediction

For the global structure inference network, we have tested the performance without AUC loss, projected depth images, and global context modeling. In addition, we also tested global models that only take CSDF or BSurf as input to figure out the importance of different input channels. We also tried to replace the 1x1x1 convolutional layer of the global network with an encoder-decoder. For intuitive comparison, Fig. 3 shows all the outputs for a sampled chair model.

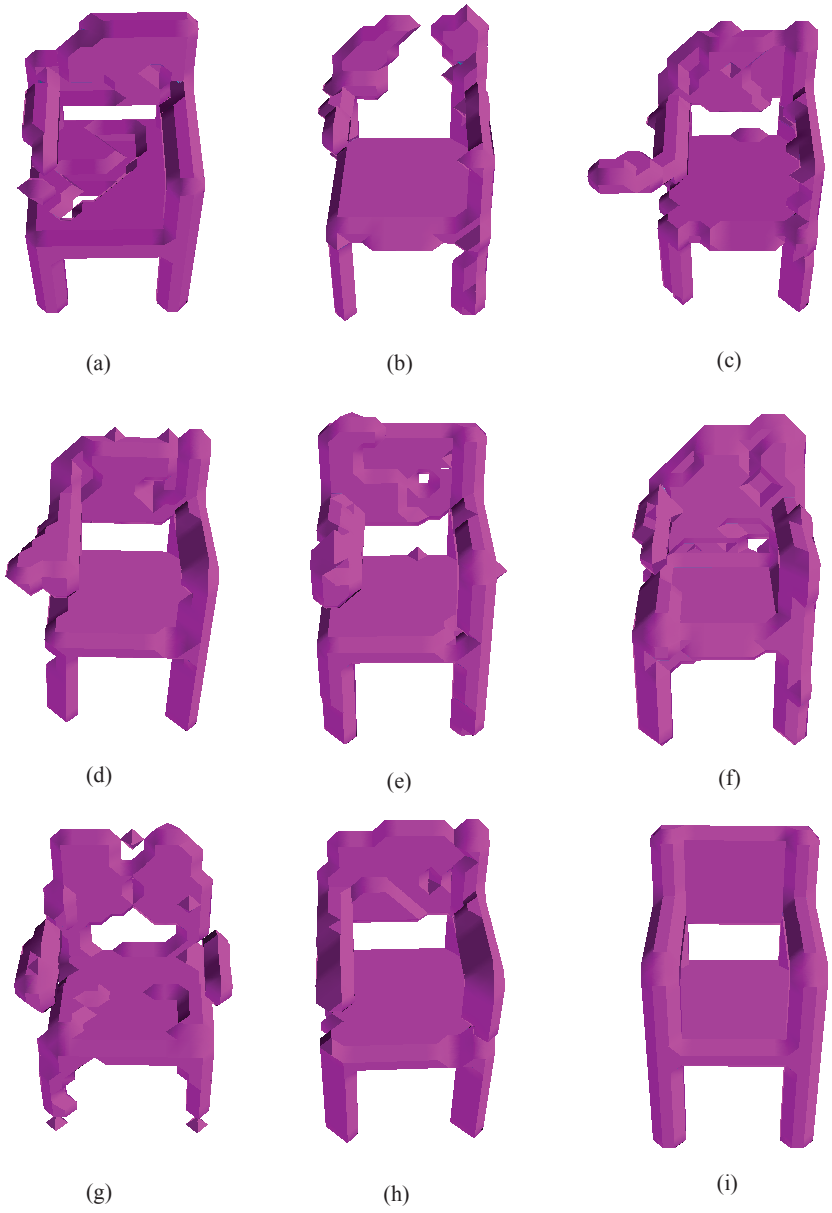

Figure 3. Sampled outputs from ablation study of global structure network. (a) is input. (b)-(h) are outputs of w/o AUC loss, w/o depth images, w/o BLSTM context modeling, w/o BSurf channel, BSurf channel only, replacing the 1x1x1 convolution layer with an encoder-decoder and the complete global network, respectively. (i) is the ground-truth global structure.

4. Comparisons with Poisson Reconstruction

To verify the efficiency of our algorithm, we conduct comparisons against Poisson surface reconstruction [1]. We show comparison results of 5 sampled models in Fig. 4, one model per row. For each model, we show the input, the high-resolution completion result of our algorithm, the output of Poisson surface reconstruction [1] and the ground-truth side by side.

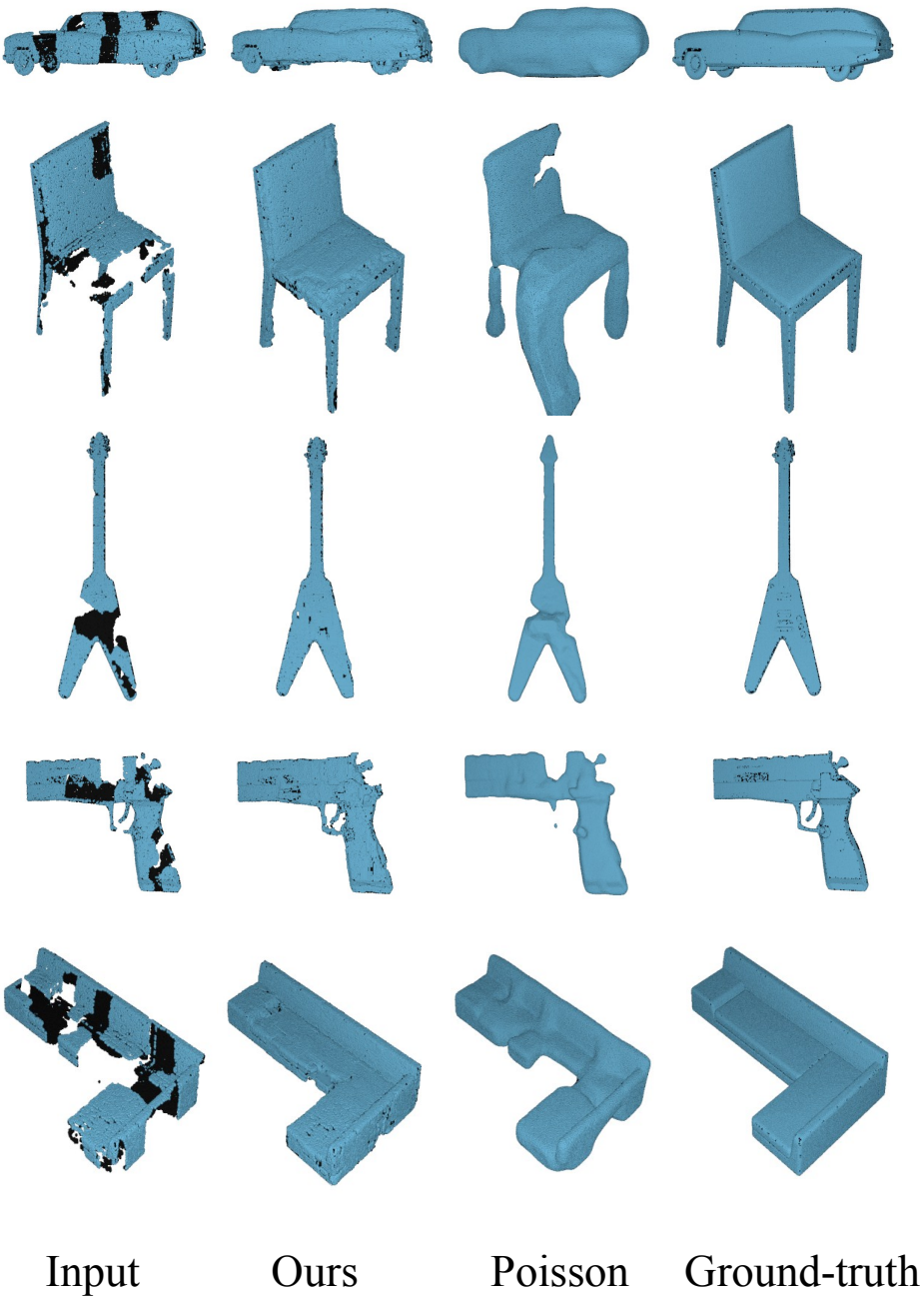

Figure 4. Sampled comparison results with Poisson reconstruction method [1].

5. More High-Resolution Shape Completion Results

Here, we also show more high-resolution shape completion results in Fig. 5– Fig. 10, one figure per object category.

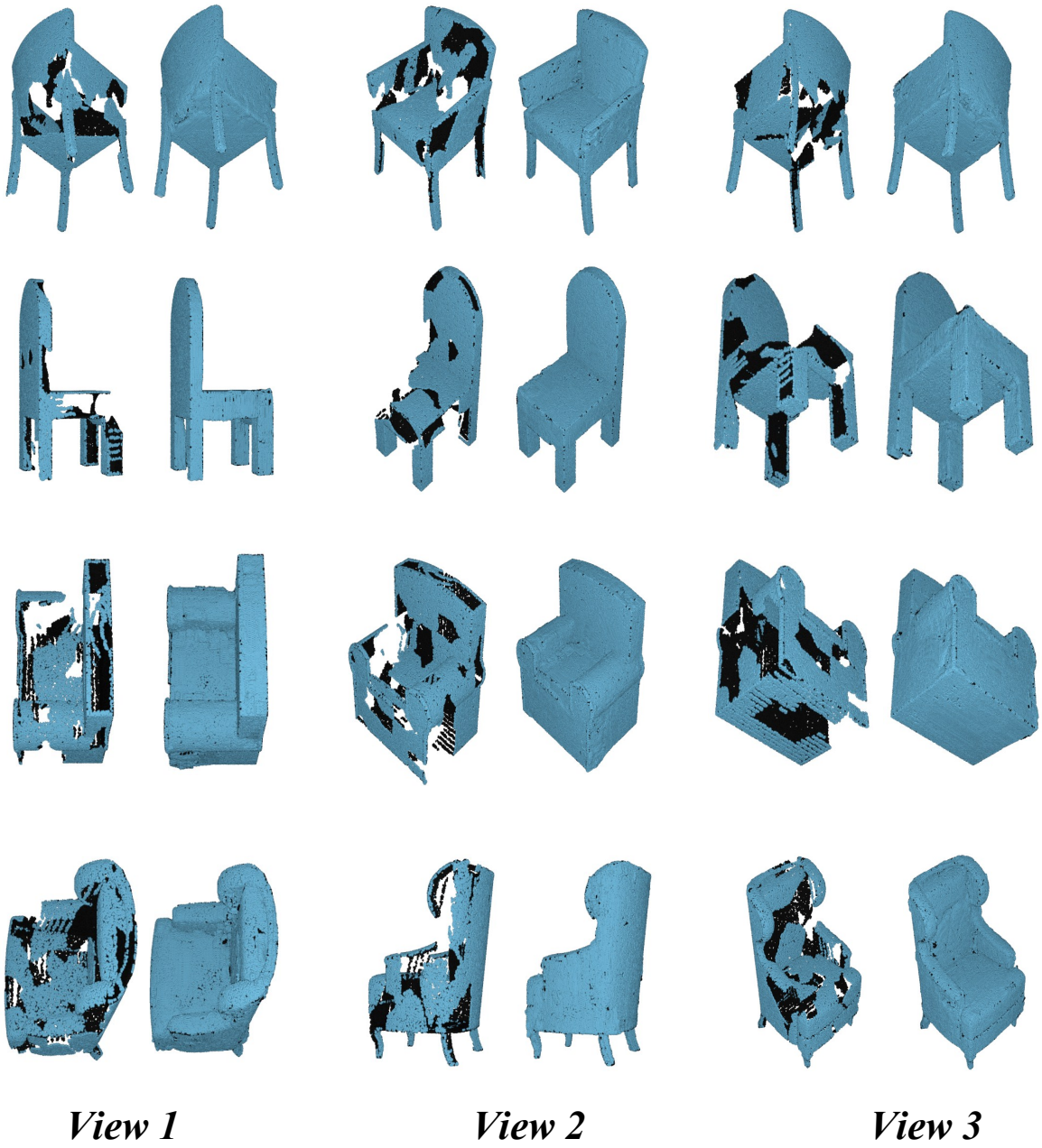

Figure 5. Gallery of completion results for the 'chair' category. One model per row. The input and repaired point clouds are shown side by side from three different views.

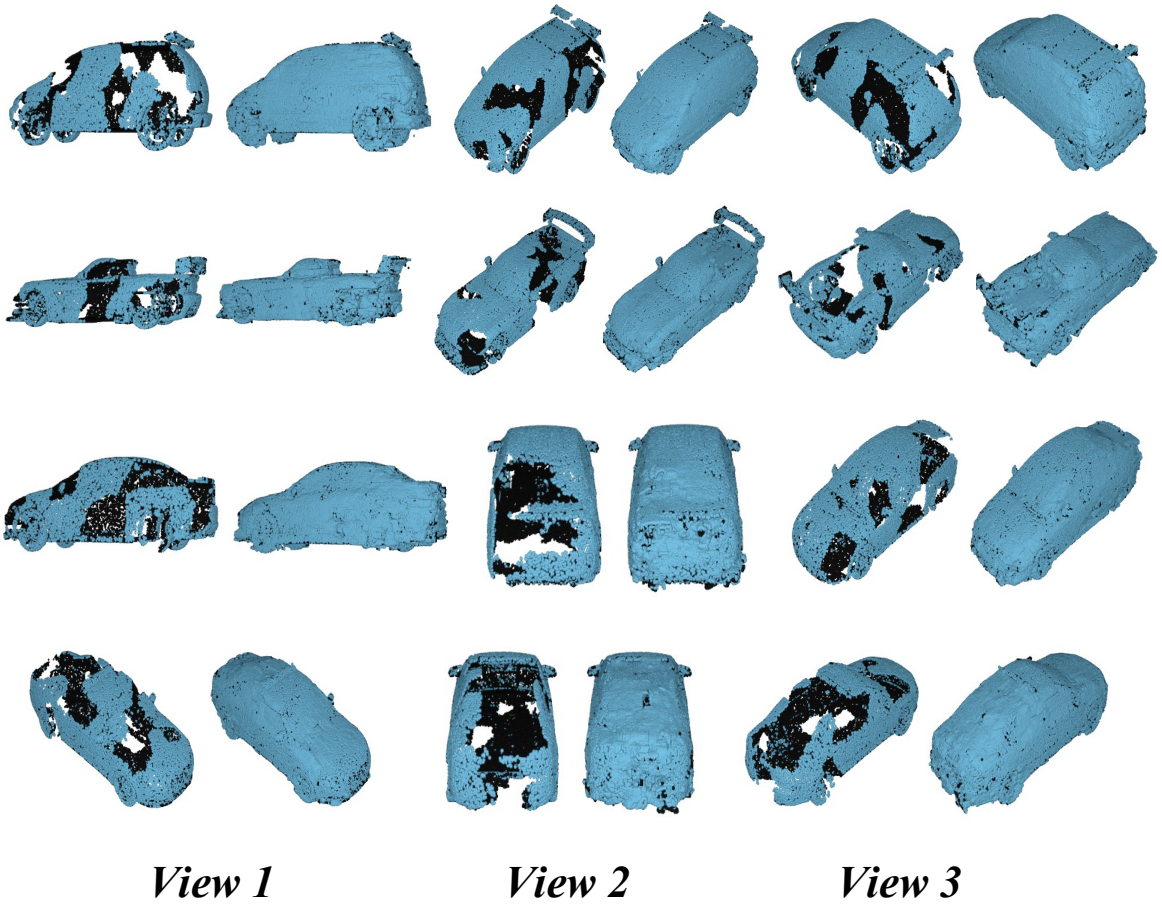

Figure 6. Gallery of completion results for the 'car' category. One model per row. The input and repaired point clouds are shown side by side from three different views.

6. Shape Completion for larger missing regions

To verify the effectiveness of our algorithm on point clouds with larger missing regions, we re-generated training and testing data and re-trained our joint learning model for the 'chair' category. In this new setting, each partial shape is generated from one or two nearby, randomly selected viewpoints simulating scanning with a real depth sensor, and typically has an entire side missing. The average completeness of an input point cloud is only 55.68%. The average completeness and normalized dist of a completed model are 91.67% and 0.00459 respectively. The F1-score of our global network reaches 0.895 and the F1-score of our local refinement network reaches 0.951, both only slightly lower than the ones for point clouds scanned from 3-5 viewpoints. The completion results for two sampled models are shown in Fig. 11.

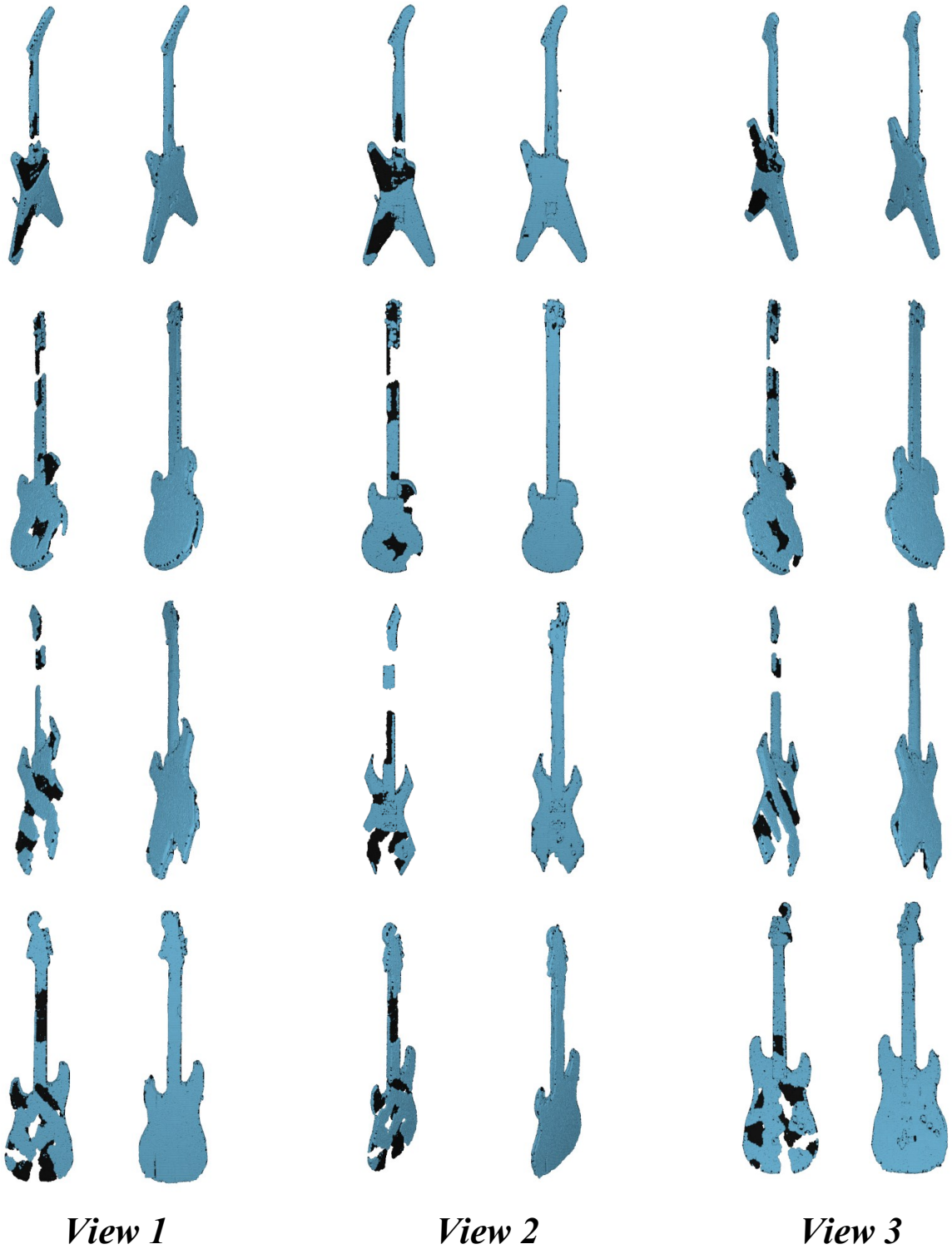

Figure 7. Gallery of completion results for the 'guitar' category. One model per row. The input and repaired point clouds are shown side by side from three different views.

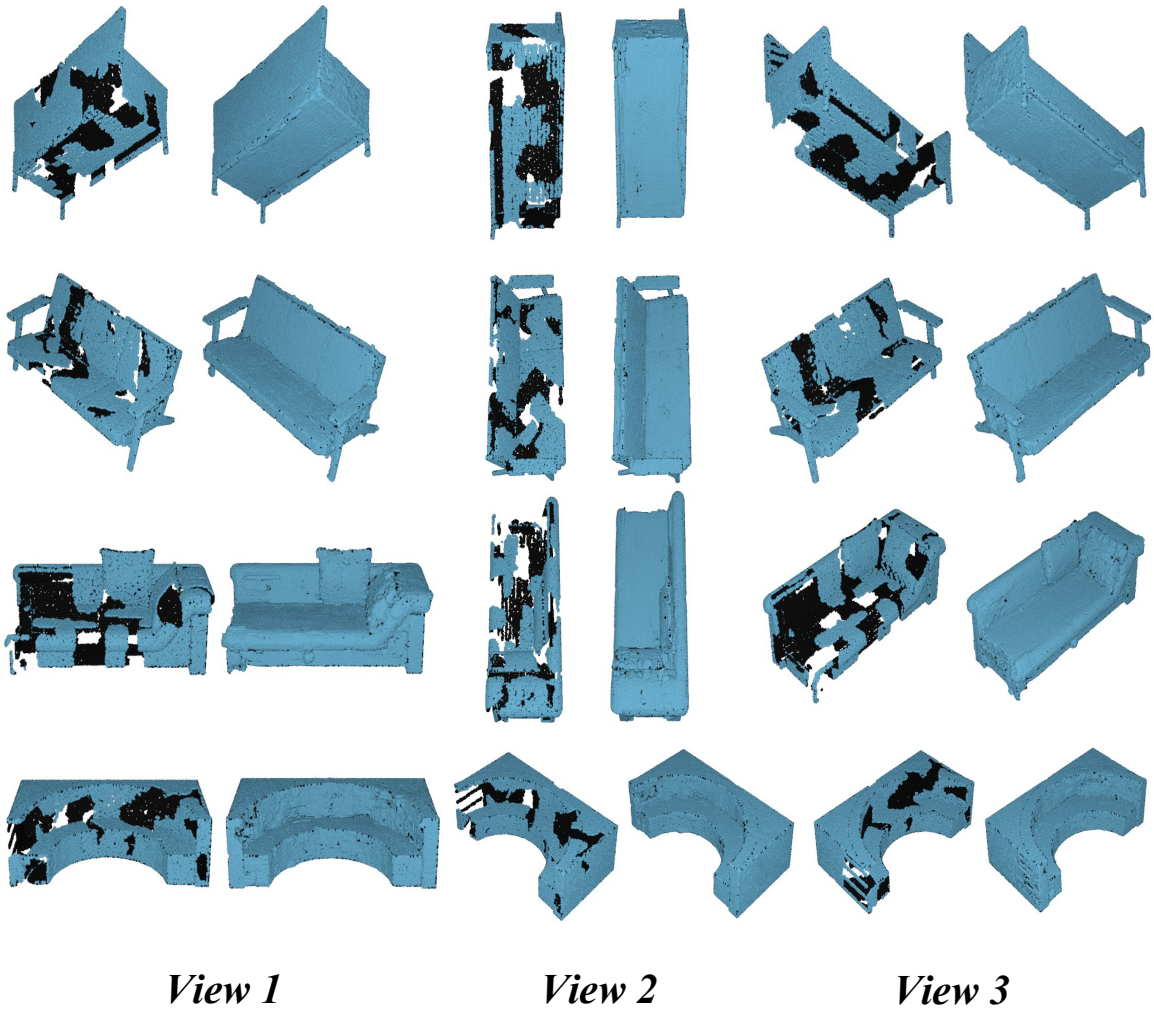

Figure 8. Gallery of completion results for the 'sofa' category. One model per row. The input and repaired point clouds are shown side by side from three different views.

Figure 9. Gallery of completion results for the 'gun' category. One model per row. The input and repaired point clouds are shown side by side from three different views.

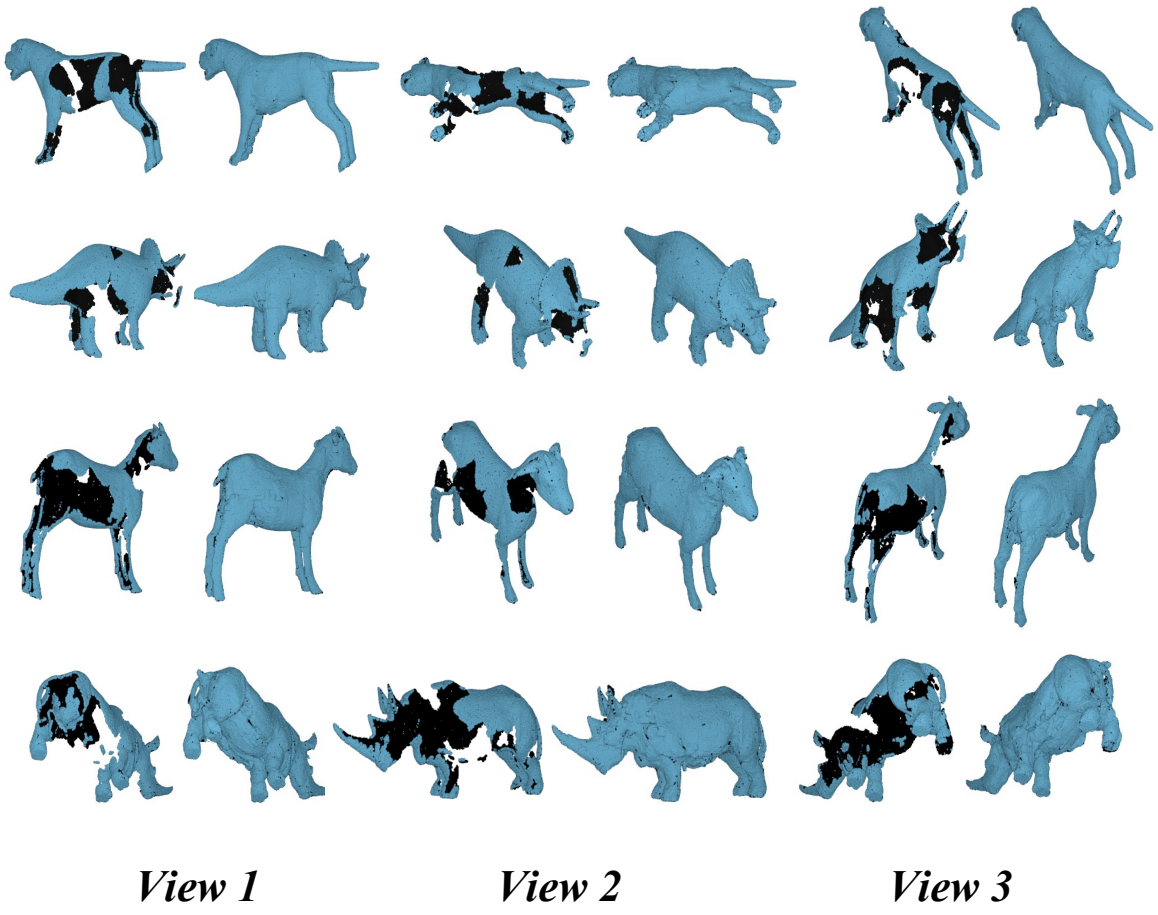

Figure 10. Gallery of completion results for 'animal' category. One model per row. The input and repaired point clouds are shown side by side from three different views.

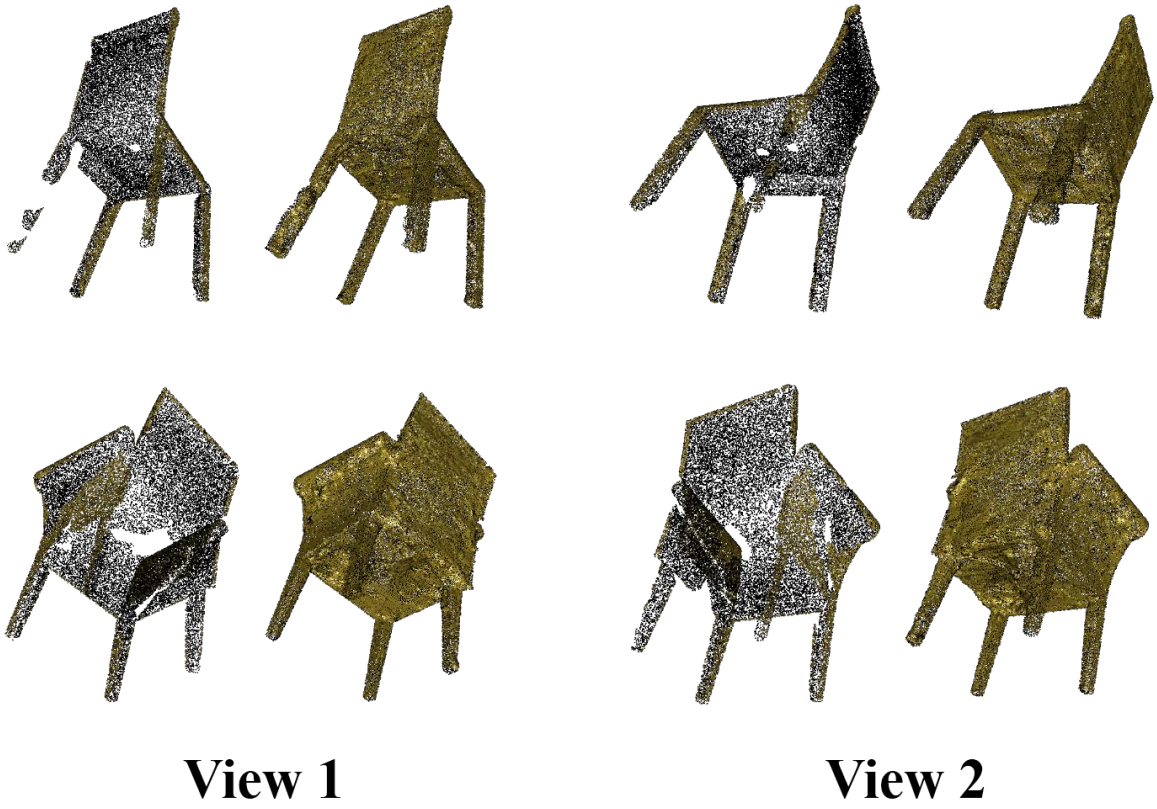

Figure 11. Two completion results for two sampled models with large missing regions (one side is entirely missing). One model per row. The input and repaired point clouds are shown side by side from two different views.

References

[1] M. Kazhdan, M. Bolitho, and H. Hoppe. Poisson surface reconstruction. In *Proceedings of the fourth Eurographics symposium on Geometry processing*, volume 7, 2006. 4